Carbohydrate Polymers 98 (2013) 1–7

Contents lists available at SciVerse ScienceDirect

Carbohydrate Polymers

journal homepage: www.elsevier.com/locate/carbpol

Properties of aqueous solutions of lentinan in the absence and presence of zwitterionic surfactants

Leandro G. Nandi, João P.T.A. Guerra, Ismael C. Bellettini, Vanderlei G. Machado, Edson Minatti*

Departamento de Química, Universidade Federal de Santa Catarina, UFSC, Florianópolis, SC 88040-900, Brazil

ARTICLE INFO

Article history:
Received 22 March 2013
Received in revised form 11 April 2013
Accepted 13 April 2013
Available online 8 May 2013

Keywords:
Polysaccharides
Helix-coil transition
Lentinan
SAXS
Zwitterionic surfactants

ABSTRACT

Morphological and conformational transitions of lentinan (**LT**), a β-glucan extracted from Shiitake mushrooms (*Lentinula edodes*), were investigated at different concentrations of aqueous NaOH, using Small Angle X-ray Scattering (SAXS) technique. At low $NaOH_{(aq)}$ concentration **LT** chains are self-associated and adopt the triple helix form where as at higher NaOH concentrations the polymer chains undergo a transition to random coil chains. Also, the presence of fractal dimensions was observed through analysis of the exponential decay of the scattering intensity as a function of the scattering angle. In addition, the lateral radius of gyration was determined for **LT** in different concentrations of NaOH solution, indicating a rigid triple helix present as a small rod-like structure. Interactions of **LT** with two zwitterionic surfactants were investigated by surface tension, fluorescence, and static light scattering measurements. Experimental data showed that the formation of **LT**–(surfactant) complexes occurred through a cooperative process.

1. Introduction

The study of biopolymers has grown considerably in recent decades because of their wide application in different areas and relatively low cost. In addition, such polymers have low impact on the environment, since they are biodegradable and biocompatible. The polysaccharides produced by algae, bacteria and fungi have been extensively used in technological applications (Silva et al., 2006). β-Glucans, polysaccharides of high molecular weight extracted from the cell walls of edible mushrooms, are used in medicine due to their bioactive, immunomodulatory and antitumor properties (Zhang, Cui, Cheung, & Wang, 2007). Lentinan (**LT**), one such polysaccharide, has a high molecular weight (5×10^5 g mol^{-1}) and contains only D-glucopyranose units in its macromolecular structure, with mostly β-(1→3)-glucose linkages in its regularly branched backbone and β-(1→6)-glucose side-chains (Zong, Cao, & Wang, 2012) (Fig. 1).

In aqueous solution, **LT** is self-associated in the form of triple helix chains (Xu, Wang, Cai, & Zhang, 2010; Xu, Zhang, Zhang, & Wu, 2004). It is known that this triple helix conformation is maintained due to intra- and intermolecular hydrogen bonding in aqueous solution (Zhang, Zhang, & Xu, 2004). This conformation changes when **LT** is dissolved in dimethyl sulfoxide (Wang et al., 2009; Wang, Zhang, Zhang, & Ding, 2009) or if the temperature is increased (Zhang, Xu, & Zhang, 2008). Likewise, it can alter when **LT** is dissolved in aqueous NaOH: a triple helix string formation occurring at concentrations of NaOH below 5×10^{-2} mol L^{-1} and a random conformation being observed at concentrations of NaOH greater than 8×10^{-2} mol L^{-1} (Zhang et al., 2004).

A better understanding of the morphological transitions of β-glucans such as **LT** is an important prerequisite to assessing the relationship between bioactivity and morphology, since a number of biological and immune pharmacological activities described in the literature are dependent on the conformation of these polysaccharides (Surenjav et al., 2005; Wasser & Weis, 1999). Sakurai et al. (2005) have shown that β-glucans with β-(1→3)-glucose linkages, for instance, **LT**, curdlan and schizophyllan, form macromolecular complexes with polynucleotides, such as DNA and RNA, and also interact with other molecules and conjugated polymers forming nanocomposites (Li, Zhang, Xu, & Zhang, 2011; Liu, Xu, Zhang, & Yu, 2012).

Many studies on the relationship between the molecular conformation and antitumor activity of **LT** and other β-glucans have been reported (Tang et al., 2012; Zong et al., 2012), but little is known about the interaction of **LT** with amphiphilic molecules and its behavior in the presence of such molecules. In this context, in this study, we extracted **LT** from the fruiting bodies of Shiitake mushrooms (*Lentinula edodes*). After the characterization of **LT**, its morphological structure was investigated at different concentrations of aqueous NaOH by means of the Small Angle

* Corresponding author. Tel.: +55 48 3721 6844; fax: +55 48 3721 6852.
E-mail addresses: edson.minatti@ufsc.br, eminatti@gmail.com (E. Minatti).

0144-8617/$ – see front matter © 2013 Elsevier Ltd. All rights reserved.
http://dx.doi.org/10.1016/j.carbpol.2013.04.053

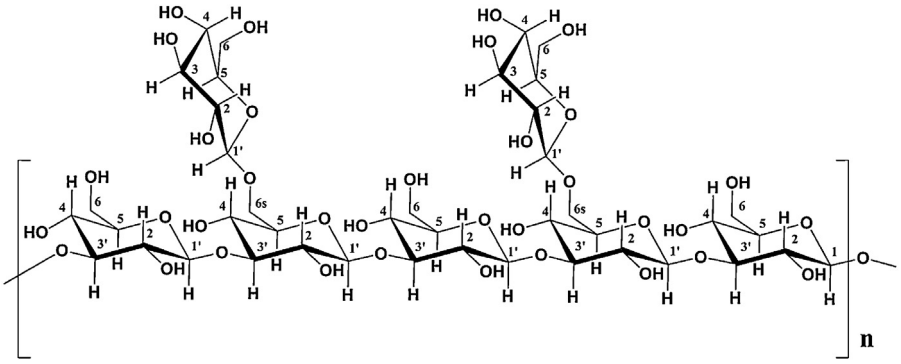

Fig. 1. Representation of the chemical structure of **LT**.

X-ray Scattering (SAXS) technique. Subsequently, the interaction of **LT** with the zwitterionic surfactants *N*-dodecyl-*N*,*N*-dimethyl-3-ammonio-1-propanesulfonate (SB3–12) and *N*-tetradecyl-*N*, *N*-dimethyl-3-ammonio-1-propanesulfonate (SB3–14) was investigated in aqueous solutions through surface tension, fluorescence, and static light scattering (SLS) measurements.

2. Experimental

2.1. Materials

SB3–12 and SB3–14 were supplied by Sigma–Aldrich with a purity of 99%, and were used without further purification. Pyrene (Sigma–Aldrich, 99%) was recrystallized three times from methanol and dried before use. The deionized water used in all measurements was obtained through previous distillation, followed by purification employing a Millipore Milli-Q system.

2.2. Characterizations

The Fourier transform infrared (FT-IR) spectra of **LT** were recorded with an ABB FTLA 2000 spectrophotometer. For each sample 100 scans were recorded at between 4000 and 600 cm^{-1}, with a resolution of 4 cm^{-1} using KBr pellet. The ^{13}C NMR spectrum was recorded on a Varian NMR AS 400 spectrometer operating at 100 MHz. This spectrum was obtained in DMSO-d_6 solution with an **LT** concentration of 4×10^{-2} g mL^{-1} at 25.0 °C.

For all solutions used in the SAXS studies the **LT** concentration was kept constant at 1.0 mg mL^{-1}. The concentration of NaOH was varied with each sample. Each sample was prepared 24 h prior to testing and kept under constant stirring for complete dissolution of the polysaccharide. For all aqueous solutions used in the study of the **LT**–surfactant interactions, the concentration of **LT** was maintained constant at 0.5 mg mL^{-1}. All solutions prepared were left to stand for at least two hours before use.

2.3. Extraction of *LT*

The polysaccharide was extracted using the methodology described by Yap (Ann-Teck Yap & Ng, 2001). Fresh shiitake mushroom caps (200.0 g) were mixed with 1.0 L of distilled water and homogenized in a blender. The resultant mixture was placed in a 2.0 L round-bottomed flask and refluxed for 24 h. The mixture was then filtered and the volume of the filtrate was reduced by distillation to 300 mL. The remaining solution was added to an equal volume of absolute ethanol, and the gelatinous precipitate formed was filtered. The precipitate was dissolved in 100.0 mL of water at 80.0 °C under stirring and filtered to remove insoluble matrices. This process was repeated three times. Finally, the sample was dissolved in 50 mL of a solution of NaOH (1.0 mol L^{-1}) and placed in a dialysis membrane (Spectra/Por® 6, *MWCO* = 3500 g mol^{-1}) and dialyzed for seven days. Finally, the resulting aqueous solution was lyophilized, yielding 0.115 g of solid white flakes. IR (KBr, $\bar{\nu}_{max}/cm^{-1}$): 3410 (O–H stretching), 2920 (CH_2 stretching), 1638 (O–H bending), 1370 (CH_2 bending), 1161 (C–O–C stretching), 1078 (C–H β-1→6 glycosidic linkages), 1041 (C–H β-1→3 glycosidic linkages), and 890 (C–H bending). ^{13}C NMR (100 MHz, DMSO-d_6) δ/ppm: 103.9 (C1,C1′), 73.5 (C2), 87.0 (C3), 77.4 (C3′), 69.1 (C4), 76.3 (C5), 71.5 (C6), 70.6 (C6s).

2.4. SAXS measurements

All SAXS studies were carried out on the D11A-SAXS beamline of the Brazilian Synchrotron Light Laboratory (LNLS – Campinas – Brazil). The wavelength (λ) of the incoming beam was set at 0.1488 nm and the samples were injected into a 1 mm-thick sample (Cavalcanti et al., 2004). The collimated beam crossed the samples through an evacuated flight tube ($p < 0.1$ mbar) and scattered to a 2D CCD mar CCD detector with an active area of 16 cm^2. The sample-detector distance was set at 1479.75 mm (silver behenate was used for the calibration of the sample-to-detector distance due to its well-known lamellar structure, $d = 58.48$ Å). The q range covered at this distance was 0.10–2.3 nm^{-1}. 2D-images were found to be isotropic and were corrected by taking into account the dark noise of the detector and normalized by the sample transmission. These images of the samples were subtracted from the corrected and normalized 2D image of the solvent, and the resulting images were then azimuthally integrated, considering the 360° scan to generate the final I as a function of q profiles. This procedure was performed with the use of the FIT2D software developed by Hammersley (Hammersley, 2009).

2.5. Surface tension data

Surface tension measurements were performed using the du Noüy ring method, at 25.0 ± 0.1 °C on a Kruss K8 GMBH interfacial tensiometer equipped with a Pt-Ir-20 ring. The ring was rinsed with a hydrochloric acid solution (4.0 mol L^{-1}) and then with deionized water several times before each measurement. The critical micellar concentration (*cmc*) as well as the critical aggregation concentration (*cac*) and polymer saturation point (*psp*) in aqueous solution were estimated from the intersections between the two linear portions of the surface tension *versus* log *c*(surfactant) plots.

2.6. Steady-state fluorescence

The steady-state fluorescence emission spectra for pyrene were recorded on a Hitachi F4500 spectrofluorimeter equipped with a thermostated cell holder set at 25.0 ± 0.1 °C and the samples were continuously stirred in a quartz cell of 10 mm path length. The

Table 1
Comparison between ^{13}C NMR chemical shift data for **LT** in DMSO-d_6 obtained in this study and literature data.

	δ/ppm							
Sample	C1 C1′	C2	C3	C3′	C4	C5	C6	C6s
Wang and Zhang (2009)	103.3	73.4	86.8	77.1	68.5	76.3	61.2	70.5
Zhang et al. (2002)	103.1	72.9	86.3	76.8	68.5	76.2	61.0	70.1
This study	103.9	73.5	87.0	77.4	69.1	76.3	61.5	70.6

probe concentration was fixed at 1.0×10^{-6} mol L^{-1} to avoid the formation of pyrene microcrystals and extrinsic phenomena. Both slit width settings of excitation and emission monochromators were adjusted to 2.5 nm. The samples were excited at 336 nm and the emission spectra were recorded from 360 to 500 nm. The following procedure was applied for all experiments performed. The fluorescence spectrum was recorded after the addition of each volume of surfactant solution. The I_1/I_3 ratio was considered as the ratio between the maximum band emission intensities of the probe at 372.8 nm (I_1) and 384.0 nm (I_3).

2.7. Static light scattering (SLS) measurements

The apparent molecular weight ($M_{W,app}$), radius of gyration (R_g) and the second virial coefficient (A_2) of **LT** were determined by the Zimm plot method (Burchard, 2008; Schärtl, 2007; Wang & Zhang, 2009) using a BI-MwA light scattering spectrometer (Brookhaven Instruments Corporation) and a laser of 620.0 nm at angles of 35, 50, 75, 90, 105, 135, and 145°. Pure toluene was used to obtain the optical constants for the equipment. The differential index of refraction (dn/dc) was determined in a BI-DNDC differential refractometer (Brookhaven Instruments Corporation) at 620.0 nm, with DNDCW Windows™ software. Stock solutions of **LT** were prepared in 2.0×10^{-2} mol L^{-1} of NaOH under magnetic stirring for at least 12 h. The dn/dc value was 1.45×10^{-4} L g^{-1}.

The **LT**–SB3–12 and **LT**–SB3–14 solutions were prepared from an aqueous solution containing 0.5 mg mL^{-1} of **LT**, with the surfactant concentration increasing from 0.10 to 3.25 mmol L^{-1} for SB3–12 and from 0.01 to 0.25 mmol L^{-1} for SB3–14. The measurements were taken at a temperature of 25.0 ± 0.1 °C, analyzing the scattering intensity at an angle of 90°. All these solutions were optically purified by filtration through Millipore filters with a pore size of 0.45 μm.

3. Results and discussion

3.1. Characterization of *LT*

The FT-IR spectrum of **LT** (Figure S1) showed a broad band at 3410 cm^{-1} characteristic of O–H stretching, bands at 1078 and 1041 cm^{-1} corresponding to C–H β-1→6 glycosidic and β-1→3 glycosidic linkages, respectively, and a band at 890 cm^{-1} associated with C–H bending, the latter being typical of β-D-glucose in pyranose form (Wang et al., 2009; Wang, Zhang, et al., 2009). The absence of a band at 850 cm^{-1} demonstrated that there were no α-glycosidic linkages in the structure of **LT** (Surenjav, Zhang, Xu, Zhang, & Zeng, 2006; Wang et al., 2009; Wang, Zhang, et al., 2009; Yu et al., 2010; Zhang, Zhang, & Cheng, 1999). The ^{13}C NMR spectrum for **LT** was collected in DMSO-d_6 solution (Figure S2). Table 1 shows a comparison between the chemical shifts obtained in this study and other data reported in the literature (Wang & Zhang, 2009; Zhang, Li, Zhou, Zhang, & Chen, 2002), which indicates that the data are very similar, indicating that **LT** was isolated and confirming its high purity.

The values for $M_{W,app}$ (9.41×10^5 and 9.69×10^5 g mol^{-1} for $c = 0$ and $\theta = 0$, respectively), R_g (154.0 nm), and A_2 (1.01×10^{-3} mL mol g^{-2}) for LT were determined in aqueous solution of NaOH (2.0×10^{-2} mol L^{-1}) by the Zimm plot method (Figure S3) (Burchard, 2008; Schärtl, 2007; Wang & Zhang, 2009). The $M_{W,app}$ and R_g values are in agreement with data previously reported by Xu et al. (2010) and Maeda, Hamuro, and Chihara (1971). The positive value of A_2 indicates that an aqueous solution of NaOH (2.0×10^{-2} mol L^{-1}) is a good solvent for LT, because the polymer–solvent interactions are stronger than the polymer–polymer interactions (Schärtl, 2007).

3.2. SAXS measurements

LT was investigated in aqueous solution by means of the SAXS technique, keeping a constant polymer concentration of 1.0 g L^{-1}. These studies were performed in order to evaluate possible morphological differences in **LT** in aqueous solution at different NaOH concentrations. The interpretation of the angle dependence of the intensity of X-ray scattering is simplified when fractal geometry is used to describe the **LT** structure. The intensity of SAXS for fractal objects is given by Eq. (1) (Guinier & Fournet, 1955; Sorensen & Wang, 1999):

$$I(q) = I_0(q)^{-a} \quad (1)$$

Thus, when the system has a fractal structure, a linear region with slope-α is observed in the plot of log $I(q)$ as a function of log(q). If $1 < \alpha < 3$, the region is the result of a fractal volume (mass or pores) and if $3 < \alpha < 4$ the region is the result of a fractal surface, and the geometry of the basic repeating unit of the fractal is directly correlated to the slope α, as established in Table S1, adapted from the literature (Burchard, 2008; Schärtl, 2007; Stribeck, 2007).

SAXS measurements for **LT** powder can be described by Porod's Law, corresponding to the classical Euclidean geometry, with an α value of 4 (Figure S4) and domains exhibiting smooth surfaces and sharp density transitions (Stribeck, 2007). Fig. 2 shows the angle

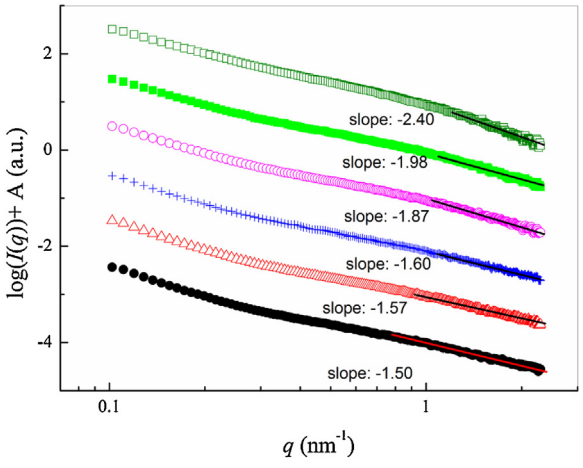

Fig. 2. The double logarithmic plot of the scattering intensity $I(q)$ *versus* the magnitude of scattering vector q for 1.0 mg mL^{-1} in the absence (□) and in the presence of 20.0 (■), 40.0 (○), 60.0 (+), 80.0 (Δ), and 100.0 (●) mmol L^{-1} $NaOH_{(aq)}$ at 25 °C. Each one of the scattering curves was vertically shifted by a factor *A*.

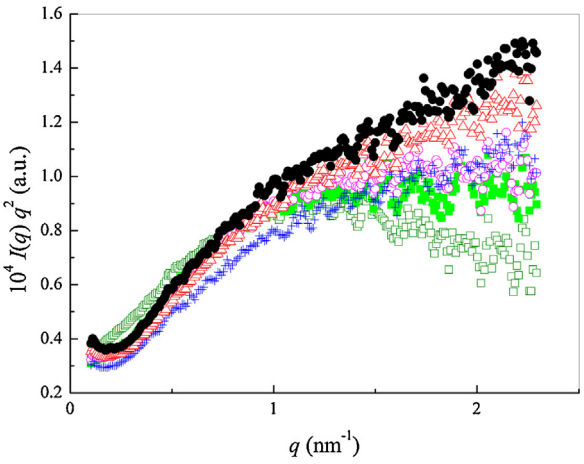

Fig. 3. Kratky plots of **LT** in the absence (□) and in the presence of 20.0 (■), 40.0 (○), 60.0 (+), 80.0 (Δ), and 100.0 (●) mmol L^{-1} $NaOH_{(aq)}$ at 25.0 °C. c(**LT**) = 1.0 mg mL^{-1}.

dependence of the scattering intensity log($I(q)$) as a function of q for **LT** in the absence of $NaOH_{(aq)}$ and with different $NaOH_{(aq)}$ concentrations (20.0, 40.0, 60.0, 80.0, and 100.0 mmol L^{-1}). As shown in Fig. 2, the angle dependency of the scattering intensity varies from $q^{-1.98}$ to $q^{-1.50}$ when the NaOH concentration is 20.0 or 100.0 mmol L^{-1}, respectively. The α values were within the limits of a fractal volume region. According to Table S1, the increase in the c(NaOH) leads to changes in the fractal dimension of the polymer, ranging from values close to 2.0 (solvated branched polymer) to values close to 5/3 (Gaussian coil). This suggests, as described by other authors using different techniques, a transition of the **LT** morphology from triple helix to random coil chains (Xu, Xu, Zhang, & Zhang, 2008; Zhang et al., 2004) when the c(NaOH) is increased.

Fig. 3 shows the Kratky plot ($I(q)q^2$ as a function of q) (Tada, Matsumoto, & Masuda, 1998) of an aqueous solution of **LT** in the absence of NaOH and in the presence of increasing c(NaOH) at 25.0 °C. The rigidity of the association of molecular chains can be estimated from the Kratky plot (Gawronski, Conrad, & Stahmann, 1996; Svergun & Feĭgin, 1987; Tada et al., 1998). In the case of a Gaussian coil, the curves do not exhibit any plateau. On the other hand, for a rigid rod particle, the scattering curves increase with increasing q until reaching a plateau (Gawronski et al., 1996).

The Kratky plots for **LT** systems ranging from 0.0 mmol L^{-1} to *ca.* 60.0 mmol L^{-1} of NaOH show a clear plateau, which approximated the behavior of rod-like particles. On the Kratky plot for the system containing 80.0 and 100.0 mmol L^{-1} the scattering intensity increased with q and a plateau was not observed. This behavior is characteristic of Gaussian coil chains.

These experimental results suggest that the conformation of the molecular chains of **LT** gradually changes from rod (triple helix) to random coil (single helix) with an increase in c(NaOH). This transition is promoted by $NaOH_{(aq)}$, resulting in the disruption of inter- and intramolecular hydrogen bonds that hold together the **LT** chains, in the form of a triple helix (Zhang et al., 2004).

In order to gain further insight in to the fine structure of the rod-like molecular self-association of **LT** at lower c(NaOH) in aqueous solution, the cross-section radius for the rod-like structure was estimated with the use of SAXS data. The Guinier approximation for the scattering intensity of the cross-section moiety provides the radius of gyration for the cross section of the rod-like particle

Table 2
R_{gc} values for **LT** at different NaOH concentrations at 25.0 °C. The concentration of **LT** was 1.0 mg mL^{-1}.

c(NaOH) (mmol L^{-1})	R_{gc} (Å)
0.0	8.0
20.0	6.5
40.0	6.0
60.0	5.3
80.0	[a]
100.0	[a]

[a] At high NaOH concentrations, the formalism for a rod can no longer be applied to the system, because **LT** chains, at c(NaOH) ≥ 80.0 mmol L^{-1}, are found in the random coil form.

(R_{gc}, the lateral radius of gyration), according to Eq. (2) (Gawronski et al., 1996; Sun, 2004; Svergun & Feĭgin, 1987; Tada et al., 1998).

$$I_c(q) = I_0(q)\ \exp\left(-\frac{R_{gc}^2 q^2}{2}\right) \quad (2)$$

Therefore, the curves of $\ln I(q)q$ as a function of q^2 (Figure S5) were used to estimate the R_{gc} values using Eq. (2). In Table 2 it can be observed that the R_{gc} values obtained decreased with an increase in the c(NaOH). This trend may be attributed to the conformational modification of **LT**, which gradually changes from the triple-helix to the single-helix chain (random coil) conformation, as mentioned above.

3.3. Surface tension measurements

Fig. 4 shows the surface tension values for SB3–12 and SB3–14 in the absence and in the presence of 0.5 mg mL^{-1} of **LT** in aqueous solutions. In the absence of **LT** the SB3–12 profile shows a net break occurring at 37.6 mN m^{-1}, which gives the critical micellar concentration (*cmc*) value of 2.20 mmol L^{-1}, while the SB3–14 profile shows a net break occurring at 37.7 mN m^{-1}, leading to *cmc* = 0.31 mmol L^{-1}. These values are in good agreement with those found by other authors (Graciani, Rodríguez, Muñoz, & Moyá, 2005) using the same technique. In the presence of **LT**, the surfactant profiles exhibit discontinuities followed by two constant regions. A first narrow plateau at 42.0 mN m^{-1} for SB3–12 and 41.7 mN m^{-1} for SB3–14 is now observed, corresponding to the onset of the binding of the SDS micellar clusters to the polymer. This is known as the critical aggregation concentration (*cac*) (Norwood, Minatti, & Reed, 1998; Zanette, Felippe, Schweitzer, Dal Bó, & Lopes, 2006) and was at 0.75 mmol L^{-1} for SB3–12 and 0.09 mmol L^{-1} for SB3–14. Above this point the surface tension decreases again until reaching a plateau. At this point, which is referred to as the polymer saturation point (*psp*), the **LT**–surfactant association ends, being interpreted as the SB3–12 or SB3–14 concentration at which the saturation of the **LT** chain with the surfactant monomers is complete (Zanette et al., 2006). The *psp* occurs at 2.0 mmol L^{-1} for SB3–12 and at 0.29 mmol L^{-1} for SB3–14, and after this point the surface tension values remain constant at 37.6 mN m^{-1} for both surfactants in the absence and presence of the polymer.

3.4. Fluorescence measurements

The technique of fluorescence measurements using pyrene as a fluorescent probe has been widely employed in the investigation of micelles (Eising et al., 2008; Kalyanasundaram, Graetzel, & Thomas, 1975; Zana, 1986), in lipophilic environments (Glushko, Karp, & Sonenberg, 1976; Glushko, Thaler, & Karp, 1981), in solvation studies (Kusumoto, Takeshita, Kurawaki, & Satake, 1997; Silva, da Silva, Machado, Longhinotti, & Frescura, 2002) and in

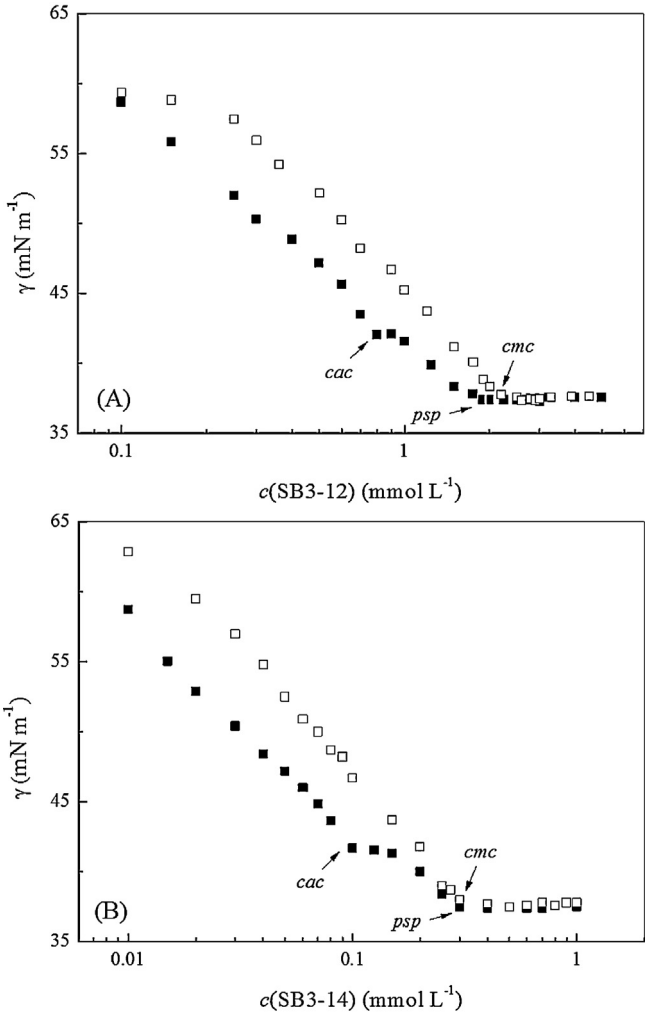

Fig. 4. Surface tension plots for SB3–12 (A) and SB3–14 (B) in the absence (□) and in the presence (■) of **LT** (0.5 mg mL^{-1}) at 25.0 ± 0.1 °C. The *cmc*, *cac* and *psp* are indicated with arrows (and described in the text).

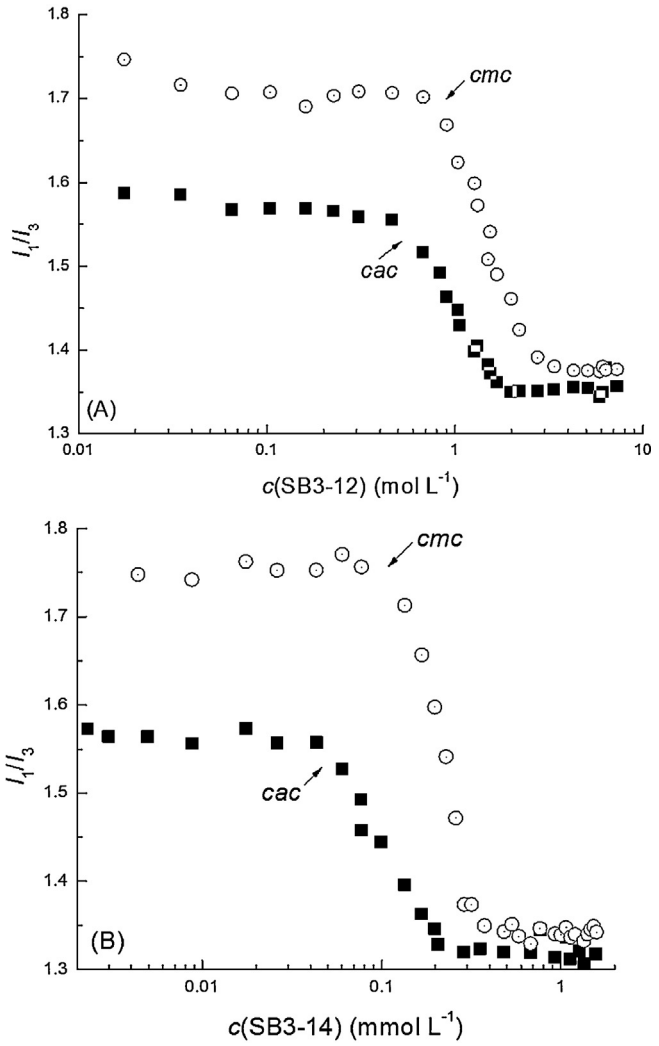

Fig. 5. Influence of I_1/I_3 ratio on the fluorescence emission of pyrene in aqueous solutions containing increasing amounts of SB3–12 (A) and SB3–14 (B) in the absence (○) and in the presence (■) of **LT** (c(**LT**) = 0.5 mg mL^{-1}). The pyrene concentration was 1.0×10^{-6} mol L^{-1}, with excitation at 336 nm, and the excitation and emission slits were adjusted to 2.5 nm at 25.0 ± 0.1 °C.

the investigation of aqueous mixtures of polymers and surfactants (Bellettini et al., 2012; Felippe, Bellettini, Eising, Minatti, & Giacomelli, 2011). Pyrene is used as a probe due to the fact that the intensities of its emission vibronic bands are strongly dependent on the medium polarity (Kalyanasundaram & Thomas, 1977; Nakajima, 1971). More precisely, an increase in the intensity of the first fluorescence emission band (I_1) occurs in the presence of polar solvents, while only a slight effect occurs in the case of the third band (I_3) (Kalyanasundaram & Thomas, 1977; Nakajima, 1971). The I_1/I_3 ratio has been used in a scale of solvent polarities (Dong & Winnik, 1982): a value of 1.8 was observed for water and 0.6 for hexane. Polarity changes in the microenvironment of the probe are reflected in an alteration in the I_1/I_3 ratio.

Fig. 5 shows plots of the I_1/I_3 ratio for the fluorescence of pyrene as a function of the concentrations of SB3–12 and SB3–14, in the absence and in the presence of **LT** at a fixed concentration of 0.5 mg mL^{-1}. The I_1/I_3 ratio in the presence of very small amounts of SB3–12 or SB3–14 is around 1.75, which is consistent with the water polarity (Dong & Winnik, 1982). The *cmc* values could be determined considering the surfactant concentration where the upper plateau ends. According to this methodology, the *cmc* values for SB3–12 and SB3–14 were determined as 1.05 and 0.15 mmol L^{-1}, respectively. These *cmc* values are lower than those obtained based on the surface tension, and this occurs because the low pyrene solubility in water can lead to the occurrence of pre-micellar aggregates (Zanette et al., 2006), which induces the formation of micelles.

With the presence of **LT** in the SB3–12 or SB3–14 systems the profile is shifted considerably and the upper plateau ends at lower SB3–12 and SB3–14 concentrations. The data for the **LT**–SB3–12 system clearly show the *cac* to be 0.62 mmol L^{-1}, and those for **LT**–SB3–14 show a *cac* of 0.06 mmol L^{-1}. Likewise, the addition of **LT** to the SB3–12 and SB3–14 solutions led to a shift in the *cmc* values toward a lower concentration. Hence, the presence of a *cac* in both systems indicates the formation of **LT**–SB3–12 and **LT**–SB3–14 complexes through a cooperative process.

3.5. SLS measurements

SLS data are shown in Fig. 6 for the titration of SB3–12 and SB3–14 in the absence and in the presence of **LT**. In these experiments the SLS intensity was monitored at an angle of 90° in the solutions as a function of the surfactant concentration. It can be observed that the data related to the **LT**–SB3–12 (Fig. 6A) and **LT**–SB3–14 (Fig. 6B) systems are similar: the addition of surfactant causes an increase in the SLS intensity in the region corresponding

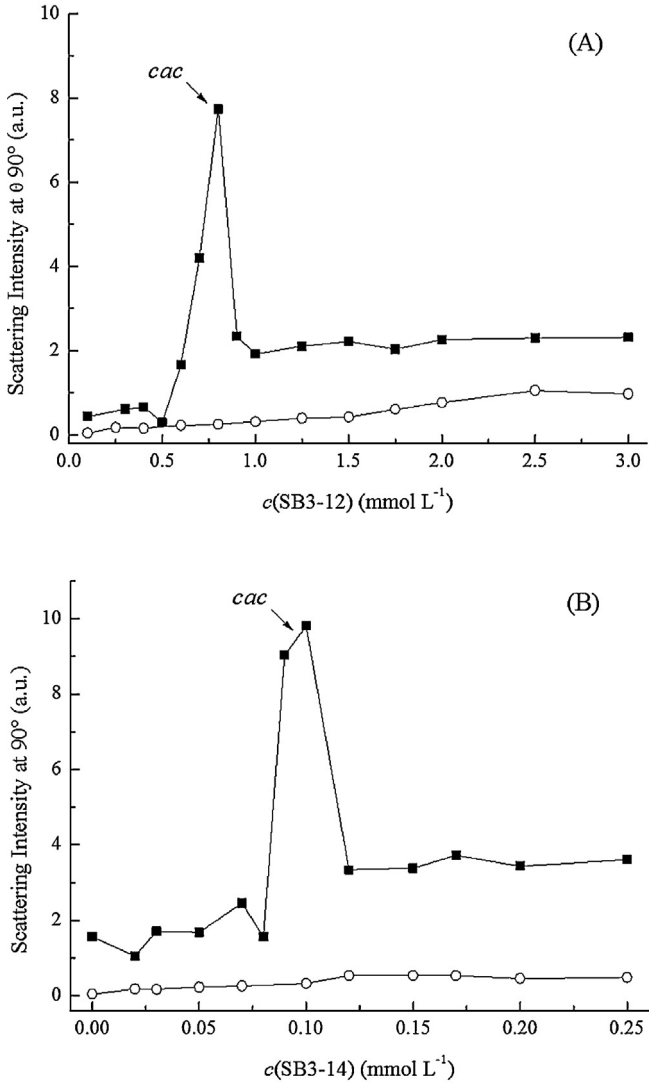

Fig. 6. Plots of SLS intensity at θ 90° of SB3–12 (A) and SB3–14 (B) in the absence (○) and in the presence (■) of **LT** (c(**LT**) = 0.5 mg mL^{-1}).

to the *cac* for each system. This provides evidence of the formation of polymer–surfactant complexes.

At low surfactant concentration the SLS intensity is low, reaching a maximum which characterizes the onset of **LT**–surfactant association. The *cac* values obtained for **LT**–SB3–12 and **LT**–SB3–14 were 0.80 and 0.10 mmol L^{-1}, respectively. These results suggest that at the *cac* (corresponding to the maximum scattering) the **LT** triple chains are swelled through interaction with surfactant molecules. If more surfactant is added, the triple chains are broken down into single chains, decorated with surfactant molecules, leading to smaller objects and therefore to a decrease in the scattering intensity. In other words, the surfactant promotes the morphological transition (triple to single chains) of **LT**. The **LT** chain saturation (*psp*) occurs at higher surfactant concentrations, and from this point onward the micelles of free surfactant are observed to be in equilibrium together with the **LT**–surfactant complexes in solution.

4. Conclusions

SAXS data revealed that **LT**, when in the solid state, has a structure that follows Porod's Law, with domains presenting smooth surfaces and sharp density transitions. However, when in water, **LT** shows a fractal organization (fractal volume) similar to small rods and the fractal dimension shifts to smaller values upon the addition of aqueous NaOH, indicating a change in the polymer structure to a single chain random coil conformation. Another important factor is that the R_{gc} values for **LT** were obtained for the first time. These data allowed a better understanding of the nature of the conformational transition of **LT**, since in the absence of NaOH the R_{gc} value for the biopolymer is 8.0 Å (triple helix) and in the presence of c(NaOH) = 60.0 mmol L^{-1} this value decreases to R_{gc} = 5.3 Å, indicating a gradual transition to single random coil chains.

Also, the interaction of **LT** with SB3–12 and SB3–14 was verified through surface tension, pyrene fluorescence and SLS measurements. Through these techniques the *cmc* values of the surfactants were determined and *cac* and *psp* values were obtained for the **LT**–SB3–12 and **LT**–SB3–14 systems. The data obtained in this study suggest that the **LT**–surfactant interactions occur *via* cooperative associations.

Acknowledgements

The authors acknowledge the Brazilian Synchrotron Light Laboratory (LNLS) for the beamtime under proposal SAXS1 – 9363 and SAXS1 – 12478, UFSC, and the Brazilian government agency Conselho Nacional de Desenvolvimento Científico e Tecnológico (CNPq) for financial support.

Appendix A. Supplementary data

Supplementary data associated with this article can be found, in the online version, at http://dx.doi.org/10.1016/j.carbpol.2013.04.053.

References

Ann-Teck Yap, & Ng, M.-L. (2001). An improved method for the isolation of lentinan from the edible and medicinal shiitake mushroom *Lentinus edodes* (Berk.) Sing. (Agaricomycetideae). *International Journal of Medicinal Mushrooms*, *3*(1), 9–19.

Bellettini, I. C., Nandi, L. G., Eising, R., Domingos, J. B., Machado, V. G., & Minatti, E. (2012). Properties of aqueous solutions of hydrophobically modified polyethylene imines in the absence and presence of sodium dodecylsulfate. *Journal of Colloid and Interface Science*, *370*(1), 94–101.

Burchard, W. (2008). Light scattering from polysaccharides as soft materials. In R. Borsali, & R. Pecora (Eds.), *Soft matter characterization* (pp. 463–603). Netherlands: Springer.

Cavalcanti, L. P., Torriani, I. L., Plivelic, T. S., Oliveira, C. L. P., Kellermann, G., & Neuenschwander, R. (2004). Two new sealed sample cells for small angle X-ray scattering from macromolecules in solution and complex fluids using synchrotron radiation. *Review of Scientific Instruments*, *75*(11), 4541–4546.

Dong, D. C., & Winnik, M. A. (1982). The Py scale of solvent polarities. Solvanet effects on the vibronic fine structure of pyrene fluorescence and empirical correlations with ET and Y values. *Photochemistry and Photobiology*, *35*(1), 17–21.

Eising, R., Morés, S., Bellettini, I. C., Felippe, A. C., Dal-Bó, A. G., & Zanette, D. (2008). Formação de micelas mistas entre o sal biliar colato de sódio e o surfactante aniônico dodecanoato de sódio. *Química Nova*, *31*, 2065–2070.

Felippe, A. C., Bellettini, I. C., Eising, R., Minatti, E., & Giacomelli, F. C. (2011). Supramolecular complexes formed by the association of poly(ethyleneimine) (PEI), sodium cholate (NaC) and sodium dodecyl sulfate (SDS). *Journal of the Brazilian Chemical Society*, *22*(8), 1539–1548.

Gawronski, M., Conrad, H., & Stahmann, K. P. (1996). Conformational changes of the polysaccharide cinerean in different solvents from scattering methods. *Macromolecules*, *29*(24), 7820–7825.

Glushko, V., Karp, C., & Sonenberg, M. (1976). The vibrational fine structure of pyrene monomer fluorescence as a probe of lipophilic environments. *Biophysical Journal*, *16*, A48.

Glushko, V., Thaler, M. S. R., & Karp, C. D. (1981). Pyrene fluorescence fine structure as a polarity probe of hydrophobic regions: Behavior in model solvents. *Archives of Biochemistry and Biophysics*, *210*(1), 33–42.

Guinier, A., & Fournet, G. (1955). *Small-angle scattering of X-rays* (1st ed., pp.). New York: Wiley.

Graciani, M. D., Rodríguez, A., Muñoz, M., & Moyá, M. L. (2005). Micellar solutions of sulfobetaine surfactants in water-ethylene glycol mixtures:surface tension, fluorescence, spectroscopic, conductometric, and kinetic studies. *Langmuir*, *21*(16), 7161–7169.

Hammersley, A. P. (2009). *Scientific software FIT2D*. Grenoble: European Synchrotron Research Facility.

Kalyanasundaram, K., Graetzel, M., & Thomas, J. K. (1975). Electrolyte-induced phase transitions in micellar systems. Proton and carbon-13 nuclear magnetic

resonance relaxation and photochemical study. *Journal of the American Chemical Society*, *97*(14), 3915–3922.
Kalyanasundaram, K., & Thomas, J. K. (1977). Environmental effects on vibronic band intensities in pyrene monomer fluorescence and their application in studies of micellar systems. *Journal of the American Chemical Society*, *99*(7), 2039.
Kusumoto, Y., Takeshita, Y., Kurawaki, J., & Satake, I. (1997). Preferential solvation studied by the fluorescence spectrum of pyrene in water–alcohol binary mixtures. *Chemistry Letters*, *26*(4), 349–350.
Li, S., Zhang, Y., Xu, X., & Zhang, L. (2011). Triple helical polysaccharide-induced good dispersion of silver nanoparticles in water. *Biomacromolecules*, *12*(8), 2864–2871.
Liu, Q., Xu, X., Zhang, L., & Yu, J. (2012). Interaction between polydeoxyadenylic acid and β-glucan from *Lentinus edodes*. *European Polymer Journal*, *48*(7), 1329–1338.
Maeda, Y. Y., Hamuro, J., & Chihara, G. (1971). The mechanisms of action of antitumour polysaccharides. I. The effects of antilymphocyte serum on the antitumour activity of lentinan. *International Journal of Cancer*, *8*(1), 41–46.
Nakajima, A. (1971). Solvent effect on the vibrational structures of the fluorescence and absorption spectra of pyrene. *Bulletin of the Chemical Society of Japan*, *44*(12), 3272–3277.
Norwood, D. P., Minatti, E., & Reed, W. F. (1998). Surfactant/polymer assemblies. 1. Surfactant binding properties. *Macromolecules*, *31*(9), 2957–2965.
Sakurai, K., Uezu, K., Numata, M., Hasegawa, T., Li, C., Kaneko, K., et al. (2005). β-1,3-Glucan polysaccharides as novel one-dimensional hosts for DNA/RNA, conjugated polymers and nanoparticles. *Chemical Communications*, *35*, 4383–4398.
Schärtl, W. (2007). *Light scattering from polymer solutions and nanoparticle dispersions* (1st ed., pp.). Berlin: Springer.
Silva, M. A. d. R., da Silva, D. C., Machado, V. G., Longhinotti, E., & Frescura, V. L. A. (2002). Preferential solvation of a hydrophobic probe in binary mixtures comprised of a nonprotic and a hydroxylic solvent: A view of solute–solvent and solvent–solvent interactions. *The Journal of Physical Chemistry A*, *106*(37), 8820–8826.
Silva, M. d. L. C. d., Martinez, P. F., Izeli, N. L., Silva, I. R., Vasconcelos, A. F. D., Cardoso, M. d. S., et al. (2006). Caracterização química de glucanas fúngicas e suas aplicações biotecnológicas. *Química Nova*, *29*, 85–92.
Sorensen, C. M., & Wang, G. M. (1999). Size distribution effect on the power law regime of the structure factor of fractal aggregates. *Physical Review E*, *60*(6), 7143–7148.
Stribeck, N. (2007). *X-ray scattering of soft matter* (1st ed., pp.). Hamburg: Springer.
Sun, S. F. (2004). *Physical chemistry of macromolecules* (2nd ed., pp.). New York: John Wiley.
Surenjav, U., Zhang, L.-N., Xu, X.-J., Zhang, M., Cheung, P. C. K., & Zeng, F.-B. (2005). Structure, molecular weight and bioactivities of (1→3)-β-D-glucans and its sulfated derivatives from four kinds of *Lentinus edodes*. *Chinese Journal of Polymer Science*, *23*(03), 327–336.
Surenjav, U., Zhang, L., Xu, X., Zhang, X., & Zeng, F. (2006). Effects of molecular structure on antitumor activities of (1→3)-β-D-glucans from different *Lentinus edodes*. *Carbohydrate Polymers*, *63*(1), 97–104.
Svergun, D. I., & Feĭgin, L. A. (1987). *Structure analisis by small-angle X-ray and neutron scattering* (1st ed., pp.). New York: Plenum Press.
Tada, T., Matsumoto, T., & Masuda, T. (1998). Structure of molecular association of curdlan at dilute regime in alkaline aqueous systems. *Chemical Physics*, *228*(1–3), 157–166.
Tang, X.-H., Yan, L.-F., Gao, J., Yang, X.-L., Xu, Y.-X., Ge, H.-Y., et al. (2012). Antitumor and immunomodulatory activity of polysaccharides from the root of Limonium sinense Kuntze. *International Journal of Biological Macromolecules*, *51*(5), 1134–1139.
Wang, J., Xu, X., Zheng, H., Li, J., Deng, C., Xu, Z., et al. (2009). Structural characterization, chain conformation, and morphology of a β-(1→3)-D-glucan isolated from the fruiting body of Dictyophora indusiata. *Journal of Agricultural and Food Chemistry*, *57*(13), 5918–5924.
Wang, X., & Zhang, L. (2009). Physicochemical properties and antitumor activities for sulfated derivatives of lentinan. *Carbohydrate Research*, *344*(16), 2209–2216.
Wang, X., Zhang, Y., Zhang, L., & Ding, Y. (2009). Multiple conformation transitions of triple helical lentinan in DMSO/water by microcalorimetry. *The Journal of Physical Chemistry B*, *113*(29), 9915–9923.
Wasser, S. P., & Weis, A. L. (1999). Medicinal properties of substances occurring in higher basidiomycetes mushrooms: Current perspactives (review). *International Journal of Medicinal Mushrooms*, *1*, 31–62.
Xu, X., Wang, X., Cai, F., & Zhang, L. (2010). Renaturation of triple helical polysaccharide lentinan in water-diluted dimethylsulfoxide solution. *Carbohydrate Research*, *345*(3), 419–424.
Xu, X., Xu, J., Zhang, Y., & Zhang, L. (2008). Rheology of triple helical Lentinan in solution: Steady shear viscosity and dynamic oscillatory behavior. *Food Hydrocolloids*, *22*(5), 735–741.
Xu, X., Zhang, X., Zhang, L., & Wu, C. (2004). Collapse and association of denatured lentinan in water/dimethlysulfoxide solutions. *Biomacromolecules*, *5*(5), 1893–1898.
Yu, Z., Ming, G., Kaiping, W., Zhixiang, C., Liquan, D., Jingyu, L., et al. (2010). Structure, chain conformation and antitumor activity of a novel polysaccharide from *Lentinus edodes*. *Fitoterapia*, *81*(8), 1163–1170.
Zana, R. (1986). . *Surfactant solutions* (Vol. 22) New York: Marcel Dekker.
Zanette, D., Felippe, A. C., Schweitzer, B., Dal Bó, A., & Lopes, A. (2006). The absence of cooperative binding in mixtures of sodium cholate and poly(ethylene oxide) as indicated by surface tension, steady-state fluorescence and electrical conductivity measurements. *Colloids and Surfaces A: Physicochemical and Engineering Aspects*, *279*(1-3), 87–95.
Zhang, L., Li, X. L., Zhou, Q., Zhang, X. F., & Chen, R. Q. (2002). Transition from triple helix to coil of Lentinan in solution measured by SEC, viscometry, and C-13 NMR. *Polymer Journal*, *34*(6), 443–449.
Zhang, M., Cui, S. W., Cheung, P. C. K., & Wang, Q. (2007). Antitumor polysaccharides from mushrooms: A review on their isolation process, structural characteristics and antitumor activity. *Trends in Food Science & Technology*, *18*(1), 4–19.
Zhang, P., Zhang, L., & Cheng, S. (1999). Chemical structure and molecular weights of α(1→3)-β-D-glucan from *Lentinus edodes*. *Bioscience, Biotechnology, and Biochemistry*, *63*(7), 1197–1202.
Zhang, X., Zhang, L., & Xu, X. (2004). Morphologies and conformation transition of lentinan in aqueous NaOH solution. *Biopolymers*, *75*(2), 187–195.
Zhang, Y., Xu, X., & Zhang, L. (2008). Dynamic viscoelastic behavior of triple helical Lentinan in water: Effect of temperature. *Carbohydrate Polymers*, *73*(1), 26–34.
Zong, A., Cao, H., & Wang, F. (2012). Anticancer polysaccharides from natural resources: A review of recent research. *Carbohydrate Polymers*, *90*(4), 1395–1410.